









Raman spectroscopy in pure and doped zinc ferrites nanoparticles

B. Albini^{1,*} , S. Restelli¹ , M. Ambrosetti², M. Bini² , F. D'Amico³ , M. C. Mozzati¹ , and P. Galinetto¹ 

¹Department of Physics and CNISM, University of Pavia, via Bassi 6, 27100 Pavia, Italy

²Department of Chemistry, University of Pavia, viale Taramelli 16, 27100 Pavia, Italy

³ Elettra-Sincrotrone Trieste S. C. p. A, Science Park, 34149 Trieste, Italy

Received: 2 December 2022

Accepted: 12 April 2023

Published online:

25 April 2023

© The Author(s) 2023

ABSTRACT

Raman spectroscopy was applied on nanostructured ZnFe_2O_4 system in order to correlate its structural, chemical, and vibrational properties to the functional behaviour, in view of the high sensitivity of the Raman probe to the cationic order in iron oxides. In particular we investigated pure and Ga/Mg doped zinc ferrite nanoparticles synthesised by co-precipitation route by means of Raman spectroscopy with a particular focus on the correlation between their structural and magnetic properties. We firstly studied the homogeneity of the samples at the micrometer scale and their stability under laser irradiation disregarding the presence of spurious iron oxides in favour of a highly defective external shell of the nanoparticles. This hypothesis was corroborated by varying the incident laser wavelength therefore changing the investigated volume. Furthermore, we estimated the inversion degree of the spinel structure finding good agreements with the trend of the magnetic features. All the evidence found through Raman spectroscopy are supported by the results obtained with X-Ray Powder Diffraction, Electron Paramagnetic Resonance and SQUID magnetometry.

1 Introduction

ZnFe_2O_4 (ZFO) ferrite is a widely investigated system that belongs to the general class of iron oxide spinel (AB_2O_4). The arising interest in studying this kind of systems, relies on their interesting magnetic, thermal, mechanical, and electrical properties, as well as for their chemical stability. Moreover, ZFO thanks to earth abundance, easy synthesis way in

nanostructured form as well as non-toxicity of the Zn ions, is suitable to be used in different applicative fields as for instance, drug delivery, sensing [1], information storage [2], as ferrofluids [3], as magnetic resonance imaging (MRI) contrast agents and for radiofrequency magnetic hyperthermia (MH) [4]. More recently this compound seems to be also exploited as possible theranostic system and as substrate for water remediation [5] as well as in catalysis [6] and photocatalysis [7, 8].

Address correspondence to E-mail: benedetta.albini@unipv.it

Bulk ZFO is characterized by a normal spinel structure where the oxygen atoms are arranged in a close-packed face-centred cubic units network, while the divalent Zn cations (A) occupy tetrahedral sites and trivalent Fe cations (B) the octahedral ones. At the nanoregime a partial cation inversion occurs in the two sublattices and in turn nanostructured ZFO shows a mixed spinel structured in which Zn^{2+} and Fe^{3+} ions are distributed over the two sites: $(\text{Zn}_{1-x}\text{Fe}_x)^{2+}[\text{Zn}_x\text{Fe}_{2-x}]^{3+}\text{O}_4$, where x is the inversion degree, i.e., the amount of Fe^{3+} ions in the tetrahedral site, and () and [] represent the A and B sites, respectively. The cationic redistribution over the two sublattices alters the strength of the interactions between magnetic ions mediated by oxygen orbitals, thus highly affecting the magnetic properties of this compound, resulting in the appearance of a superparamagnetic behaviour at room temperature [9].

In general, the functional properties of these systems are closely depending on composition, size and architecture of the nanoparticles as well as on the synthesis methods. The general approach is to perform different doping substitution and/or to vary the synthesis methods in order to reduce particle sizes and to promote an inversion degree suitable for specific applications. This strategy, oriented to obtain e.g., a tuning of the magnetic behaviour, requires a detailed and exhaustive understanding of the structural and chemical properties and their interplay in determining functional properties. Indeed, a general issue for ZFO nanoparticles is to reveal the presence of iron oxides phases that can infer an effective, but extrinsic magnetic behaviour, causing problems in terms of stability and aggregation if used for example in biomedical applications.

A complete characterization of structural properties is usually performed by matching different methodologies, combining short- and long-range probes, optical, magnetic, electrical spectroscopies and more. This approach is time expensive and costly; thus, it is extremely important to define protocols able to quickly assess the quality of the sample.

Among the different techniques, Raman spectroscopy (RS) is certainly widely used to characterize different microscopic features of the general class of iron oxide compounds. By RS it is possible to distinguish between haematite, maghemite, magnetite and wurtzite [10]; it is possible to evaluate the stability of the phase under different laser treatments or

thermal annealing in different atmospheres. In addition, and more specifically for the spinel type structure, RS can be used to extract (semi)-quantitative information on the cationic distribution i.e., the inversion degree of the spinel. Thus, considering the sensitivity of the technique, its versatility for different sample shapes and forms, its ability to reveal unwanted spurious phases, RS seems to be a valid candidate for a quick and robust validation of the zinc ferrite sample quality once verified that spectral parameters derived from Raman experiments are directly related to functional properties.

In this work, we would like to demonstrate that Raman spectroscopy is a suitable tool to access the structural, vibrational, and chemical properties of zinc ferrite nanoparticles by exploiting the high sensitivity and the fast timescale investigation offered by the technique itself. We focused on pure and doped zinc ferrites nanoparticles synthesized through the co-precipitation method. The doping was performed on both the cationic sites by substituting Mg on Zn site and Ga on Fe site. At first, we tested the structural homogeneity within the samples and their thermal stability under laser irradiation. We also evaluated their Raman response by varying the incident laser wavelength and thus using 266, 533, 633, and 785 nm sources. Moreover, we performed semi-quantitative analyses on the ZFO Raman modes in order to get information about the cationic disorder of the spinel structure. Finally, to demonstrate the effectiveness of the Raman technique in the study of zinc ferrite, the obtained results are discussed and validated taking into account the information obtained from complementary analysis, like X-ray powder diffraction (XRPD), Electron Paramagnetic Resonance (EPR) spectroscopy and SQUID measurements, which were performed to evaluate the magnetic response.

2 Experimental

2.1 Materials and synthesis processes

For pure ZFO, $\text{Zn}(\text{NO}_3)_2 \cdot 6\text{H}_2\text{O}$ and $\text{Fe}(\text{NO}_3)_3 \cdot 9\text{H}_2\text{O}$ were dissolved in 50 ml of water, adjusting the pH value at about 10 with the addition of NaOH 2 M; in case of doping, the nitrates ($\text{Mg}(\text{NO}_3)_2 \cdot 6\text{H}_2\text{O}$ or $\text{Ga}(\text{NO}_3)_3 \cdot 8\text{H}_2\text{O}$) were added to the starting blend at the beginning of the co-precipitation procedure. The

obtained solutions were maintained at 80 °C for about 2 h, cooled down to room temperature, then centrifuged (6000 rpm for 5 min) two times with water and ethanol. The products were dried overnight at 80 °C in a muffle and finally treated at 300 °C for about 6 h to decompose the organic component. This synthesis procedure led to the formation of brownish powders with nanoparticles size of about 6–7 nm, as pointed out by the Rietveld refinement carried out on the XRPD patterns (see Table S1 in supplementary material).

The investigated samples are named as follows: ZFO for pure sample, MZFO for $\text{Zn}_{0.9}\text{Mg}_{0.1}\text{Fe}_2\text{O}_4$ and ZGFO for $\text{ZnFe}_{1.8}\text{Ga}_{0.2}\text{O}_4$.

2.2 Methods

Raman measurements were performed at room temperature (RT) using an automated and integrated confocal microRaman spectrometer, XploRA Plus HORIBA Scientific, equipped with an Olympus microscope BX43. Three different laser sources are available: 532 nm, 100 mW, 638 nm, 90 mW, and 785 nm, 100 mW. Neutral filters with different optical density allow to set incident laser power. The spectrometer is equipped with a motorized xy stage on which the investigated samples are positioned. Spectral resolution is about 1 cm^{-1} . An Open Electrode CCD camera, with a multistage Peltier air-cooling system, is used as detector.

The measurements were performed with all the three laser wavelengths, using a 50x magnification objective. Thermal cycles were performed by progressively increasing and decreasing the incident laser density power ranging from about $2.5 \times 10^6\text{ W/cm}^2$ to $2.5 \times 10^7\text{ W/cm}^2$. The spectra were acquired with a mean integration time of about 20 s and a number of accumulations equals to 10.

The UV Raman measurements were carried out with a benchtop Raman set-up at the IUVS line at the Elettra synchrotron in Trieste. A 266 nm light from a Nd:YAG laser was used as excitation source. The samples were mounted on an oscillating stage in order to avoid photo-damaging. The incident power laser was set to 200 μW . A Czerny-Turner spectrometer equipped with a holographic dispersive element of 3600 lines/mm, coupled with a Peltier-cooled back-thinned CCD has been used to record the Raman signals. The calibration of the spectrometer

was standardized using cyclohexane (Sigma-Aldrich).

EPR investigation was performed using an X-band (about 9.4 GHz) Bruker spectrometer, in the range between 2000 and 5000 G. A continuous nitrogen flow cryostat was used to carry out measurements by varying the temperature in the range between 120 and 500 K.

The magnetic characterization was carried out by means of a SQUID magnetometer. A 100 Oe magnetic field was applied to study the temperature dependence of the magnetization in the range 5–305 K, in zero-field cooling (ZFC) and field cooling (FC) regimes. Hysteresis loops were collected at room temperature and at 10 K with magnetic field ranging between 0 and $\pm 30,000$ Oe.

XRPD measurements were performed using a Bruker D5005 diffractometer with $\text{CuK}\alpha$ radiation, graphite monochromator and scintillation detector. The patterns were collected in air with a step size of 0.03° and counting time of 15s per step in the angular range $17\text{--}110^\circ$, using a silicon sample holder with low background. Rietveld structural and profile refinements were carried out by means of TOPAS 3.0 software based on the known crystal structure model of the cubic spinel.

3 Results and discussion

ZnFe_2O_4 cubic spinel belongs to the $\text{Fd}3\text{m} (O_h^7)$ space group in which the unit cell contains 8 molecules for a total of 56 atoms, but the smallest Bravais cell contains 2 formula units for a total of 14 atoms. The factor group analysis predicts five Raman active modes, namely $A_{1g} + E_g + 3F_{2g}$, however the Raman spectrum is generally dominated by three most intense peaks, namely A_{1g} , $F_{2g}(2)$ and $F_{2g}(3)$. The total symmetric mode A_{1g} generally falls between 570 and 780 cm^{-1} , the $F_{2g}(3)$ and the $F_{2g}(2)$ at about $450\text{--}500\text{ cm}^{-1}$ and $350\text{--}400\text{ cm}^{-1}$, respectively. The other two low frequency modes, E_g and $F_{2g}(1)$, could be sometimes detected and fall below 300 cm^{-1} [11]. The spectra of all the investigated samples, collected with the 638 nm laser source, are reported in Fig. 1.

As it is possible to observe, they all display the characteristic Raman features of the zinc ferrite spinel, revealing a good structural stability, also upon doping. In particular, the spectra are dominated by the A_{1g} mode. According to literature, this mode is

associated to the symmetric breathing vibration of the tetrahedron AO_4 unit where the cation is at the centre of a cube, surrounded by four oxygen atoms in the non-adjacent corners [12]. As regards the lower energy modes, a clearly stated assignation is still missing, thus in some cases they are associated to the tetrahedral cage [13] and in others to the octahedral one [14]. However, there is more accordance on the assignation of the lowest energy mode, $F_{2g}(1)$, which is due to the translational motion of the whole AO_4 unit within the spinel structure [9].

In case of doping, the presence of different cations involved in the same vibrational unit entails the broadening of the Raman features and it results in the presence of different contributions for each Raman mode. This behaviour is the so-called two-mode behaviour, and it is particular pronounced for the A_{1g} mode which is the result of the overlap of two different modes: the vibration of the ZnO_4 tetrahedral unit that produces a signal at about 650 cm^{-1} and the vibration of the FeO_4 one whose related signal is generally located at about 690 cm^{-1} [15].

The homogeneity of the zinc ferrite phase intra-sample was verified by collecting multiple automatic linear acquisition along an area of about $100\text{ }\mu\text{m}$ in different portion of the samples. As an example, the spectra collected for the pure sample are reported in Fig. S1a. As it is possible to observe, only the Raman signatures of zinc ferrite spinel dominate the spectra, with a variation in the Raman yield due to a slight loss of focus as it generally occurs in an automatic scan. The homogeneity of all the investigated samples is better highlighted in Fig. S1b, where the ratio

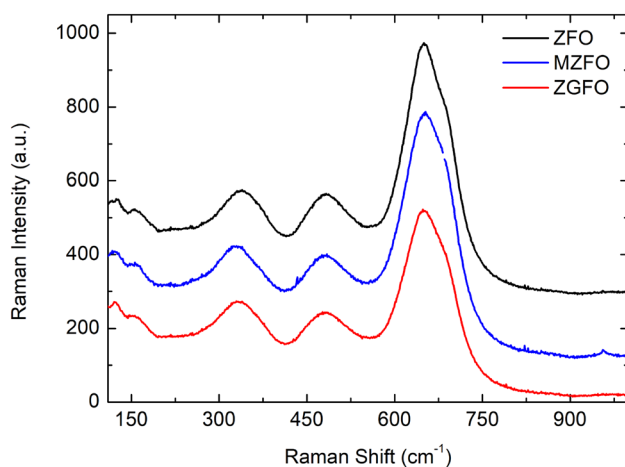
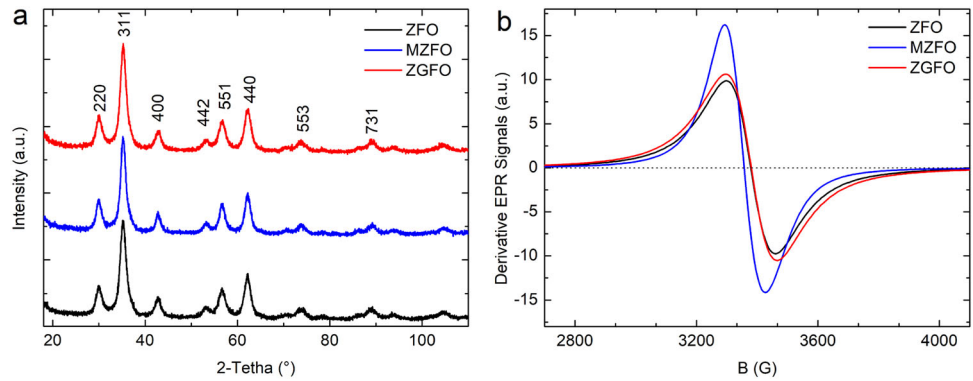


Fig. 1 Raman spectra of the investigated systems excited with a 638 nm laser wavelength

between the intensities of the A_{1g} and $F_{2g(2)}$ modes, reported as a function of the laser spot position, points out relative standard deviation (RSD) values between 12 and 17%. The resulting mean spectra are precisely reported in Fig. 1, thus demonstrating the purity of the spinel phase as confirmed by XRPD and EPR measurements. Indeed, the XRPD patterns display the typical peaks proper of the $ZnFe_2O_4$ cubic spinel structure (JCPDS card N. 89-7412, franklinite mineral) (Fig. 2a), while the room temperature derivative EPR signals present the typical broadened spectra centred around $g = 2.001$ proper of Fe^{3+} ions in paramagnetic nanostructured zinc ferrite at least for the ZFO and ZGFO samples. The MZFO sample is characterized by a room temperature EPR signal (reported in Fig. 2b) centred at $g \approx 2.01$, so not negligibly shifted with respect to the other two samples (see the comparison between the room temperature spectra reported in Fig. 2b). In general, this behaviour could be ascribed to the presence of a magnetically ordered extrinsic phase or to a SPM behaviour occurring at temperatures higher than RT. In this case, we reasonably excluded the first hypothesis in favour of the second one, since by increasing the measuring temperature the EPR signals of all the investigated samples are characterized by the same single broadened signal, observed at room temperature, without appreciable changing in the shape. Moreover, the trend of all the characteristic EPR parameters (g -factor, peak to peak linewidth, signal symmetry) is consistent with a ferrite system involved in a transition between SPM and PM states, as already shown for analogous samples in our previous contribution [16]. However, as an explanatory case, Fig. S2a reports the EPR signals collected at different temperatures for MZFO sample, while in Fig. S2b the EPR signals collected for the MZFO sample at room temperature and at 443 K are reported with comparable intensities to better highlight the lack of noticeable changes in the signal shape. This result indeed allows us to exclude the presence of other magnetically ordered iron oxide phases at least within the EPR detection limit [11].

To further investigate the purity of the sample, we verified the phase stability under laser irradiation by performing thermal cycles in different areas of each sample, as described in the sect. 2.2. The ZFO and MZFO samples display the same characteristic Raman features of the zinc ferrite spinel before and

Fig. 2 **a** XRPD patterns of the investigated samples with the Miller indices of the main reflections; **b** Room temperature derivative EPR signals of the investigated samples

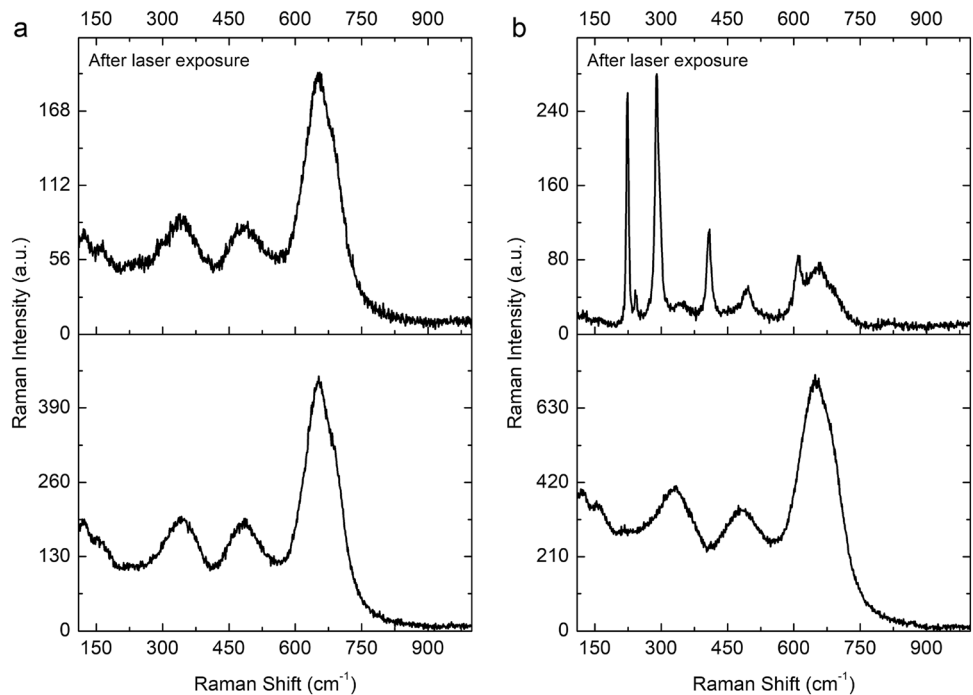


after the thermal treatment, while the ZGFO one shows different response in two different investigated areas, as shown in Fig. 3: stability under thermal treatment as well as a partial irreversible phase transition with the growth of four new peaks centred at 225, 299, 412 and 613 cm^{-1} which are characteristic of the haematite ($\alpha\text{-Fe}_2\text{O}_3$) phase. The growth of the $\alpha\text{-Fe}_2\text{O}_3$ could have two possible sources, namely (i) the presence of maghemite clusters [17] or (ii) the presence of a highly defective external shell in the ZFO nanoparticles surface [18]. Based on the presented results and, in particular, on the evidence obtained through EPR inspection, that excluded the presence of magnetically ordered extrinsic iron oxide phases, we suggest that the origin of the observed phase transformation could be plausibly traced back

to the second hypothesis, namely the presence of a highly surface defectiveness.

Thus, to deepen the investigation on the phase/structural composition gradient of the nanoparticles, we performed Raman measures by varying the incident laser wavelength and, in turn, the penetration depth of the probe itself [11]. In Fig. 4a, the comparison between the Raman spectra of ZFO sample collected with 266, 532, 638 and 785 nm light is reported in the range between 100 and 1000 cm^{-1} , where the first order Raman signal of zinc ferrite nanoparticles can be observed. Despite the difference in the intensity yield due to the different power density values used to perform the measures, and to the different scattering volumes, it is possible to observe the principal A_{1g} mode in each of the

Fig. 3 Laser-induced thermal effect on Raman spectra of ZGFO sample. The reported room temperature Raman spectra were collected at the beginning (lower figures) and at the end (upper figures) of the thermal cycle with a $2.5 \times 10^6 \text{ W/cm}^2$ incident power density, in two different regions of the sample displaying both (a) thermal stability and (b) a transition to haematite phase



reported spectra. However, some differences can be noticed for the low frequency mode; in particular, with 785 nm wavelength, the ratio of the relative intensities proper of the $F_{2g}(2)$ and A_{1g} modes is markedly different. Indeed, the two modes have almost the same Raman yield, while in the UV Raman spectrum these low frequency modes are hardly noticeable.

For the purposes of our investigation, we focused our analyses on the modifications occurring on the A_{1g} mode. Indeed, by diminishing the wavelength of the incident laser source, one can easily notice a progressively increase of the component pertinent to the Fe–O vibration in the tetrahedral unit and a corresponding lowering of the ZnO_4 component till its complete disappearance in the UV Raman spectrum. This simple observation is corroborated by the results obtained from the best-fitting procedure performed on the investigated mode and from the integrated intensity ratio (I_{Zn}/I_{Fe}) of the two components reported in Fig. 4b.

For the UV Raman spectrum the fitting procedure was performed with a single Lorentzian curve peaked at 687.2 cm^{-1} , since the component pertinent to the ZnO_4 vibration is missing. The fact that this peak is centred well below 700 cm^{-1} , namely where the maghemite mode should occur, could again support the hypothesis of a different cationic distribution from the stoichiometry ($Zn_xFe_{2-x}O_4$) in the external shell of the ZFO nanoparticles, characterized by a deficiency in Zn cations. This is consistent with the fact that with the more energetic incident source (4.66 eV) we are sensitive to a very thin outer thickness of the ZFO nanoparticles [11].

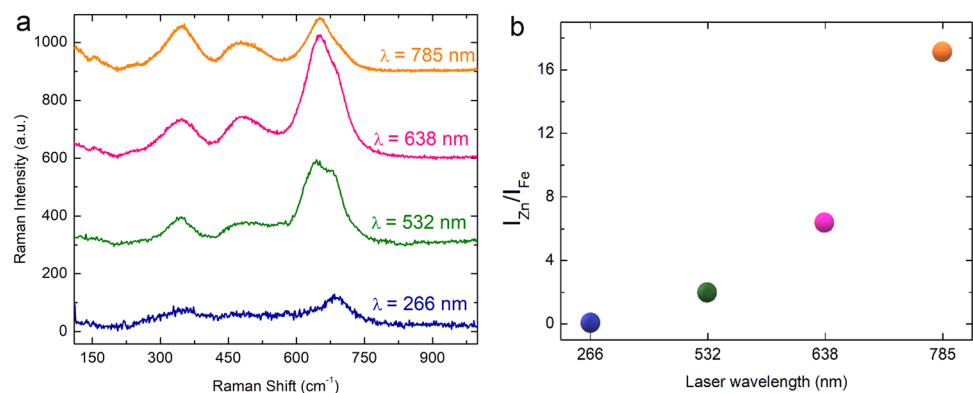
In view of this additional experimental evidence, we seem to be able to say that our samples are not affected by the presence of other iron oxides phases, at least within the detection limits of the involved techniques, being EPR the most sensitive one, and thus they could be eligible for an in-depth study on the correlation between the magnetic behaviour and the cationic disorder as derived through the RS inspection.

Indeed, as previously described, RS allows also to characterize the cationic distribution between the two sublattices which is forced at the nanoregime by exploiting the pronounced two-mode behaviour of the A_{1g} mode and thus calculating the inversion degree of the spinel structure from the following formula:

$$i.d. = 1 - \frac{I_{Zn}}{I_{Zn} + I_{Fe}}$$

Thus, we analysed the A_{1g} mode in the range between 560 and 780 cm^{-1} starting from the ZFO spectrum collected with the 638 nm source by performing a best-fitting procedure using two overlapping Lorentzian functions to take into account the two cationic vibration units in the tetrahedral site and one Gaussian function, centred out of the investigated range at about 530 cm^{-1} . The phonon confinement induced by the nanometer dimension of the particles, as well as the static disorder of cations, induced by the inversion, and of anions, due to oxygen vacancies, induce an asymmetry of the Raman lineshape [19], empirically well reproduced by adding a Gaussian curve to the fitting procedure. As it is possible to observe from Fig. 5a, the peak is well reproduced by the sum of the three fitting

Fig. 4 **a** Comparison between the ZFO Raman spectra collected with 266, 532, 638, and 785 nm laser wavelengths. **b** Ratio I_{Zn}/I_{Fe} of the integrated intensities of the two Lorentzian functions used to perform the fit on the A_{1g} mode as a function of the incident wavelengths



functions. In particular, the first Lorentzian function, centred at 647.8 cm^{-1} , gives the main contribution, while the second one, centred at 691 cm^{-1} , results in a shoulder at higher energy. These energy values are in good agreement with the ones proper of the ZnO_4 and FeO_4 unit vibrations reported in literature [9]. The inversion degree was calculated by applying the reported formula and considering only the integrated intensities of the two Lorentzian functions. The obtained value demonstrates a slight inversion of the pure spinel: $x(\text{Fe})_{\text{A}} = 0.12$.

Through this best-fitting procedure, it is possible to also evaluate the inversion degree of the other doped samples, however the presence of a dopant cation and thus an additional vibrating unit, should be considered by introducing a further Lorentzian function. This additional contribution in the best-fitting procedure is not trivial as on the other hand it is not easy, for both pure and doped nanoparticles zinc ferrites, to derive general rules for Raman modes behaviour, because several parameters, namely synthesis, grain size, composition, and chemical purity, can give rise to competing effects that reflect in opposite effects on Raman features.

In view of this complicated scenario, we propose a more simplified approach [11, 16] for the evaluation of the inversion degree of our doped samples. In particular, we evaluated the inversion degree using the same formula, but instead of using the integrated intensity, we used the heights I_1 and I_2 where the two A_{1g} mode components fall. Since the absolute value of the inversion degree obtained with this procedure is not consistent, we also evaluated the inversion degree of the pure sample with this simplified

procedure in order to normalize the two values. The normalization factor was used to rescale to the proper absolute values the inversion degree of all the doped samples.

From the reported data in Fig. 5b, it is possible to assert that the doping seems to affect the inversion, even at these low inversion degrees; in particular, the ZGFO sample results slightly less inverted, while the doping performed with the Mg ions induces more inversion in the structure if compared to the behaviour of the undoped sample. This could be consistent with the inverted spinel structure proper of the magnesium ferrite.

Since the inversion strengthens the magnetic interaction due to the presence of Fe^{3+} on both sites, from the slight value of the inversion degree one could deduce that our samples are characterized by a superparamagnetic behaviour that however is not so pronounced. Nevertheless, it is possible to infer that the Mg doping is more performant in enhancing the inversion and thus its superparamagnetic behaviour. Indeed, the EPR inspection highlights the superparamagnetic state of the MZFO sample already at room temperature.

Moreover, the inferences followed by the assessment of the inversion degree are supported by the magnetic results. Indeed, the hysteresis cycles recorded at room temperature for the three samples provided a basic proof of room temperature superparamagnetism, since the main common features ascribable to a superparamagnetic behaviour could be found (Fig. 6a): negligible values of coercive field and remanence magnetization with a no full saturation even at the highest applied magnetic

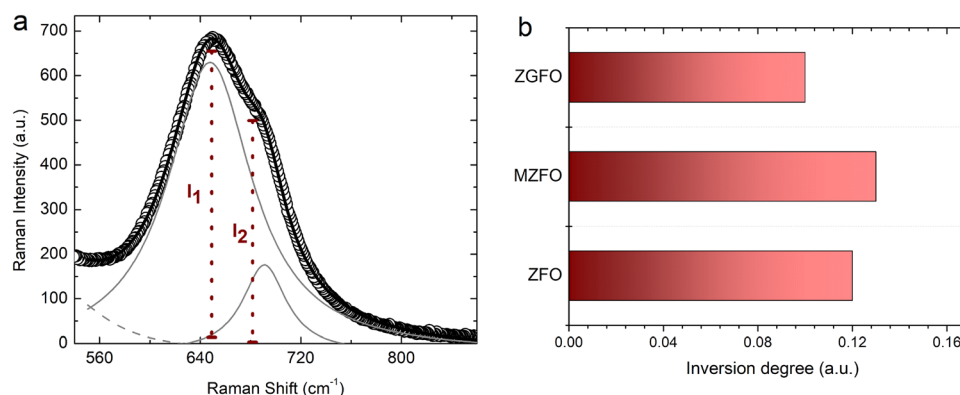


Fig. 5 **a** Best-fitting procedure performed on the A_{1g} mode for the ZFO sample, using two Lorentzian functions (solid grey lines) and a Gaussian one (dashed grey line). The brownish dotted lines

highlight the heights of the two principal components of the analysed mode. **b** Inversion degree values calculated with the simplified approach (Color figure online)

fields, typical for nanoparticles of this kind of materials.

In particular, the one proper of MZFO shows the characteristic S-type shape of a superparamagnetic behaviour, while the ZFGO and ZFO have a less pronounced one as expected from the slight inversion. Considering the obtained experimental evidence, we could state that the less marked S-type shape of the ZGFO hysteresis loop at room temperature could be ascribed to the effect of the performed doping. Indeed, the Ga ions were substituted to the Fe ones, consequently the sample has less magnetic iron centres, so the magnetic interactions could be interrupted by the presence of the dopant. This evidence also suggests that the Ga substitution tends to prevent the structural disorder of the spinel which is consistent with the lower inversion degree value estimated with Raman inspection. The temperature dependence of the magnetization (Fig. 6b) allows us to validate even more the relationship between magnetic properties and the degree of inversion of the spinel structure. The trend of the calculated inversion degree with the more simplified approach well matches the values of T_B . Indeed, the higher the inversion is, the higher the T_B value is: this is consistent with the fact that the cationic disorder within the two sublattices strengthens the magnetic interactions and, in turn, the transition to an ordered blocked state occurs at higher temperatures. Thus, the magnetic data validate the reasoning we have used to estimate the inversion degree of the spinel. Moreover, this correlation between the inversion degree and the blocking temperature has been also observed in the previously investigated samples, namely zinc ferrites characterized by Ca or Sr substitutions on the A site and Al or Gd on the B one. The results reported in [9, 16, 20] shows this

correlation except for the Sr doped sample which also presented a $\text{Sr}(\text{NO}_3)_2$ impurity phase.

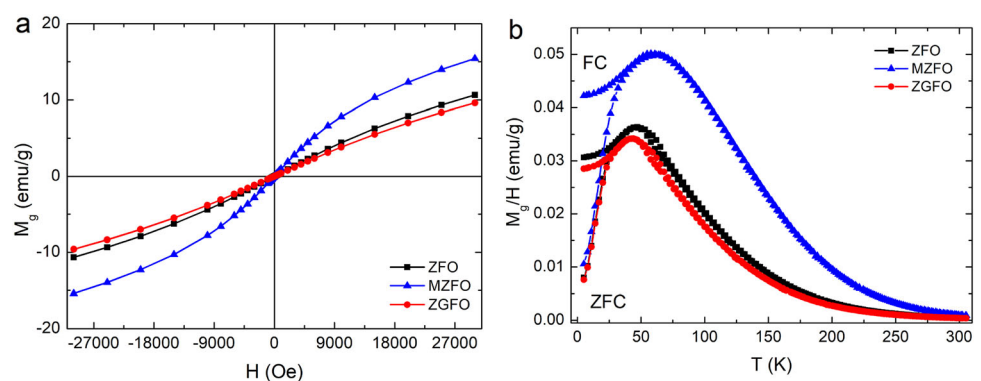
4 Conclusions

In this study, we used pure and Ga/Mg-doped zinc ferrite nanoparticles synthesised by co-precipitation route to highlight the potentiality of Raman spectroscopy as a fast and sensitive analytical tool in studying functional parameters in this kind of systems, with a particular focus on the correlation between structural and magnetic properties.

The Raman probe allowed us to evaluate the homogeneity of the samples at the micrometer scale and their stability under laser irradiation, evidencing the irreversible phase transition to the haematite phase for the ZGFO sample. At this regard, we are likely to exclude the presence of extrinsic iron oxides in favour of a highly defective external shell of the nanoparticles. This hypothesis is corroborated by the measures performed by varying the incident laser wavelength and thus by varying the probed investigated volume. Moreover, we applied a reasoned and simplified approach to estimate the inversion degree that allowed us to predict the magnetic behaviour of the current samples as well as the previous ones. All the Raman evidence was supported and endorsed by the results obtained by XRPD, EPR and magnetic measurements.

In view of the fulfilling results obtained in the presented study, the interesting functional properties of nanosized zinc ferrites as well as the intriguing overlapping between the RS characteristics and the properties of these compounds, we planned to investigate the ZFO structural, chemical and magnetic properties from a different point of view,

Fig. 6 **a** Room temperature hysteresis cycles of ZFO, MZFO, and ZGFO samples. **b** The relative ZFC and FC M vs. T curves at 100 Oe



namely on thin films deposited through RF magnetron sputtering.

Acknowledgements

For Raman experiments performed with UV light, the authors acknowledge the CERIC-ERIC Consortium for the access to experimental facilities and financial support.

Author contributions

All authors contributed to the study conception and design. Material preparation was performed by MB and MA, data collection and analysis were performed by all the authors. The first draft of the manuscript was written by BA, and all authors commented on previous versions of the manuscript. All authors read and approved the final manuscript.

Funding

Open access funding provided by Università degli Studi di Pavia within the CRUI-CARE Agreement. This research was funded by the project “CE4WE–Circular economy for Water and Energy” funded by Lombardy Region (1139857 CALL HUB 2018).

Data availability

The authors declare that the data supporting the findings of this study are available within the article. Complementary data relevant for the present study are available from the corresponding author upon reasonable request.

Declarations

Competing interest The authors have no relevant financial or non-financial interests to disclose.

Open Access This article is licensed under a Creative Commons Attribution 4.0 International License, which permits use, sharing, adaptation, distribution and reproduction in any medium or format, as long as you give appropriate credit to the original author(s) and the source, provide a link to the

Creative Commons licence, and indicate if changes were made. The images or other third party material in this article are included in the article's Creative Commons licence, unless indicated otherwise in a credit line to the material. If material is not included in the article's Creative Commons licence and your intended use is not permitted by statutory regulation or exceeds the permitted use, you will need to obtain permission directly from the copyright holder. To view a copy of this licence, visit <http://creativecommons.org/licenses/by/4.0/>.

Supplementary Information: The online version contains supplementary material available at <http://doi.org/10.1007/s10854-023-10464-0>.

References

1. S. Tajik, S.A. Ahmadi, M.B. Askari, H. Beitollahi, A sensor fabricated with spinel zinc ferrite nanoparticles and reduced graphene oxide for electrochemical detection of Sudan I. *J Iran. Chem. Soc.* **19**, 3127–3134 (2022). <https://doi.org/10.1007/s13738-022-02518-7>
2. R. Sharma, P. Thakur, P. Sharma, V. Sharma, Ferrimagnetic Ni²⁺ doped Mg-Zn spinel ferrite nanoparticles for high density information storage. *J. Alloys Compd.* **704**, 7–17 (2017). <https://doi.org/10.1016/j.jallcom.2017.02.021>
3. A.A. Ibiyemi, G.T. Yusuf, Rheological investigation of strain rate and magnetic field on the magnetorheology of zinc ferrite ferrofluid. *Appl. Phys. A* **128**, 591 (2022). <https://doi.org/10.1007/s00339-022-05720-9>
4. S.O. Aisida, A. Ali, O.E. Oyewande, I. Ahmad, A. UI-Hamid, T. Zhao, M. Maaza, F.I. Ezema, Biogenic synthesis enhanced structural, morphological, magnetic and optical properties of zinc ferrite nanoparticles for moderate hyperthermia applications. *J. Nanopart. Res.* (2021). <https://doi.org/10.1007/s11051-021-05149-w>
5. P.A. Vinosha, J.V.A. Vinsla, J. Madhavan, S. Devanesan, M.S. AlSalhi, M. Nicoletti, B. Xavier, Impact of dysprosium doped (Dy) zinc ferrite (ZnFe₂O₄) nanocrystals in photo-fenton exclusion of recalcitrant organic pollutant. *Environ. Res.* **203**, 111913 (2022). <https://doi.org/10.1016/j.envres.2021.111913>
6. P. Dave, R. Thakkar, R. Sirach, M.P. Deshpande, S. Chaturvedi, Effect of nanosize zinc ferrite on thermolysis of ammonium perchlorate. *J. Electron. Mater.* **51**(2), 785–792 (2022). <https://doi.org/10.1007/s11664-021-09335-3>
7. C. Yang, G. de Falco, M. Florent, H. Fan, M. Liang, T.J. Bandoz, The effect of ZnFe₂O₄/activated carbon adsorbent

- photocatalytic activity on gas-phase desulfurization. *Chem. Eng. J.* **423**, 130255 (2021). <https://doi.org/10.1016/j.cej.2021.130255>
8. M.P. Tsvetkov, M.M. Milanova, Z.P. Cherkezova-Zheleva, T.S. Tsoncheva, J. Ts Zaharieva, M.V. Abrashev, I.G. Mitov, Catalytic and photocatalytic properties of zinc-nickel ferrites. *J. Chem. Sci.* **133**(1), 24 (2021). <https://doi.org/10.1007/s12039-020-01882-2>
 9. P. Galinetto, B. Albin, M. Bini, M.C. Mozzati, Raman spectroscopy in zinc ferrites nanoparticles, in *Raman spectroscopy*. ed. by G.M. Do Nascimento (IntechOpen, London, 2018)
 10. D.L.A. de Faria, S. Venâncio Silva, M.T. de Oliveira, Raman microspectroscopy of some iron oxides and oxyhydroxides. *J. Raman Spectrosc.* **28**, 873–878 (1997)
 11. B. Albin, *Raman spectroscopy and nanostructured complex systems: A satisfactory win to win game?* (University of Pavia, Pavia, 2021)
 12. B.D. Hosterman (2011). Raman spectroscopic study of solid solution spinel oxides. UNLV Theses, Dissertations, Professional Papers, and Capstones. p. 1087. <https://doi.org/10.34917/2476131>
 13. T. Yamanaka, M. Ishii, Raman scattering and lattice vibrations of Ni_2SiO_4 spinel at elevated temperature. *Phys. Chem. Miner.* **13**, 156–160 (1986). <https://doi.org/10.1007/BF00308157>
 14. M. Virumbrales-del Olmo, A. Delgado-Cabello, A. Andrada-Chacón, J. Sánchez-Benítez, E. Urones-Garrote, V. Blanco-Gutiérrez, M.J. Torralvo, R. Sáez-Puche, Effect of composition and coating on the interparticle interactions and magnetic hardness of MFe_2O_4 (M=Fe, Co, Zn) nanoparticles. *Phys. Chem. Chem. Phys.* **19**(12), 8363–8372 (2017). <https://doi.org/10.1039/C6CP08743D>
 15. Z.Z. Lazarević, Č Jovalekić, V.N. Ivanovski, A. Rečnik, A. Milutinović, B. Cekić, N.Z. Romčević, Characterization of partially inverse spinel ZnFe_2O_4 with high saturation magnetization synthesized via soft mechanochemically assisted route. *J. Phys. Chem. Solids* **75**(7), 869–877 (2014). <https://doi.org/10.1016/j.jpcs.2014.03.004>
 16. G. Gazzola, M. Ambrosetti, M.C. Mozzati, B. Albin, P. Galinetto, M. Bini, Tuning the superparamagnetic effect in ZnFe_2O_4 nanoparticles with Mg, Ga doping. *Mater. Chem. Phys.* **273**, 125069 (2021). <https://doi.org/10.1016/j.matchemphys.2021.125069>
 17. Y. El Mendili, J. Bardeau, N. Randrianantoandro, F. Grasset, J. Greneche, Insights into the mechanism related to the phase transition from $\gamma\text{-Fe}_2\text{O}_3$ to $\alpha\text{-Fe}_2\text{O}_3$ nanoparticles induced by thermal treatment and laser irradiation. *J. Phys. Chem. C* **116**(44), 23785–23792 (2012). <https://doi.org/10.1021/jp308418x>
 18. J.A. Gomes, G.M. Azevedo, J. Depeyrot, J. Mestnik-Filho, F.L.O. Paula, F.A. Tourinho, R. Perzynski, Structural, chemical, and magnetic investigations of core – shell zinc ferrite nanoparticles. *J. Phys. Chem. C* **116**, 24281–24291 (2012). <https://doi.org/10.1021/jp3055069>
 19. A.K. Arora, M. Rajalakshmi, T.R. Ravindran, V. Sivasubramanian, Raman spectroscopy of optical phonon confinement in nanostructured materials. *J. Raman Spectrosc.* **38**(6), 604–617 (2007). <https://doi.org/10.1002/jrs.1684>
 20. M. Bini, C. Tondo, D. Capsoni, M.C. Mozzati, B. Albin, P. Galinetto, Superparamagnetic ZnFe_2O_4 nanoparticles: the effect of Ca and Gd doping. *Mater. Chem. Phys.* **204**, 72–82 (2018). <https://doi.org/10.1016/j.matchemphys.2017.10.033>

Publisher's Note Springer Nature remains neutral with regard to jurisdictional claims in published maps and institutional affiliations.